Stabilizing Electrolysis Cells with Oscillating Currents: Amplitude, Frequency, and Current Efficiency

Ibrahim Mohammad, Marc Dupuis, Paul D. Funkenbusch, and Douglas H. Kelley

Abstract

The metal pad instability (MPI) imposes a minimum electrolyte layer thickness for stable operation of aluminium (Al) electrolysis cells, which limits cells' energy efficiency. The MPI is a magnetohydrodynamic process that depends on a coupled resonance between hydrodynamic gravity wave modes, driven by the cell's electrolytic current, appearing as a circulating traveling wave that grows exponentially. Adding an oscillating current component, whose frequency is close to a low-frequency gravity mode instead excites standing waves that can prevent the MPI. Here, we show that a minimum oscillation amplitude is required for preventing the MPI, but excessive amplitude causes a wave that shorts the cell. Proper oscillation frequency choice also impacts the stabilization effect. We also discuss the impact of exciting standing waves on the current efficiency of the cell. Applying oscillating currents could significantly increase the energy efficiency of Al cells without the need for expensive reconstruction paving the way towards more efficient, low carbon Al production.

Keywords

Aluminium • Modeling and simulation • Low carbon technology • Magnetohydrodynamics • Sustainability

Introduction

Humankind produced 63.7 million metric tons of aluminium (Al) in 2019 [1], nearly all via the Hall-Héroult process in which electrical current liberates molten Al from dissolved alumina (Al_2O_3) in electrolysis cells. That year, Al production required 848 TWh of electricity [1], 3% of the worldwide total [2], and caused 1% [3] of the 51 Gton/year of CO_2-equivalent (CO2e) emissions produced by humankind [4]. Of those emissions, 62% originates indirectly from producing the electricity needed for electrolysis, most of which comes from coal and gas combustion [5]. Thus, improving the energy efficiency of Al production is crucial for decarbonizing the industry.

Electrolysis cells consist of two carbon electrodes, one at the anode and one at the cathode, with two shallow and broad fluid layers resting in between them: molten Al beneath a floating layer of cryolite electrolyte (bath). Ideally, all the electrical energy in an electrolysis cell should be reducing Al, however, about 40% [6] is lost as heat generated by the electrical resistance of the cell, which is concentrated at the bath since it is ∼1000 times less electrically conductive than the carbon electrodes and ∼10000 times less than the Al. This loss can be decreased by reducing the thickness of the bath, usually quantified by the anode-cathode distance (ACD).

However, squeezing the ACD below a certain critical threshold triggers a magnetohydrodynamic instability [7–13], known as the metal pad instability (MPI) [14]. The mechanism behind the MPI can be understood by first considering naturally occurring perturbations on the Al-bath interface as a superposition (sum) of many decoupled hydrodynamic gravity wave modes. In fact, the height of the Al-bath interface varies spatially and can be written in terms of the wave modes as

$$\sum_{m,n}\alpha_{m,n}G_{m,n} = \sum_{m,n}\alpha_{m,n}\cos\left(\frac{m\pi}{L_x}(x+\frac{L_x}{2})\right)\cos\left(\frac{n\pi}{L_y}(y+\frac{L_y}{2})\right) \tag{1}$$

where $G_{m,n}$ is an interface mode, $\alpha_{m,n}$ is its amplitude, (m, n) are non-negative integers, x increases along the long axis of the rectangular cell, y increases along its short axis, and $(x, y) = (0, 0)$ at the center of the cell. Each $G_{(m,n)}$ has the form of a standing wave whose temporal frequency nearly matches the corresponding hydrodynamic gravity wave mode,

I. Mohammad · P. D. Funkenbusch · D. H. Kelley (✉)
Department of Mechanical Engineering, University of Rochester, Rochester, NY 14627, US
e-mail: d.h.kelley@rochester.edu

M. Dupuis
GeniSim Inc., Jonquière, Quèbec G7S 2M9, Canada

D. Eskin (ed.), *Light Metals 2022*, The Minerals, Metals & Materials Series,
https://doi.org/10.1007/978-3-030-92529-1_73

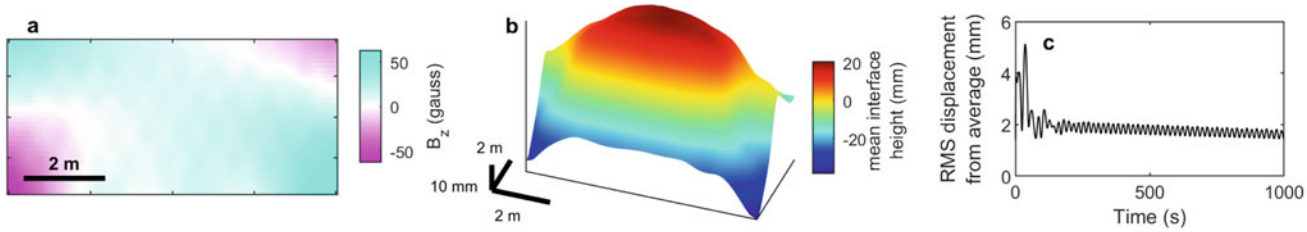

Fig. 1 Critical ACD. **a** The vertical component of the ambient magnetic field, at the Al-bath interface, from our simulations, seen from above. The field varies spatially and is caused primarily by currents in the cell and nearby busbars. **b** The Al-bath interface bulges because of electromagnetic forces due to the field and the current. The vertical axis is exaggerated to show detail. **c** The RMS displacement of the interface oscillates stably at 4.3 cm ACD

whose frequency $f_{m,n}$ [15] is independent of current and (in the limit of shallow cells) is given by

$$f_{m,n}^2 = \frac{(\rho_{Al} - \rho_c)g}{2\pi(\frac{\rho_{Al}}{h_{Al}} + \frac{\rho_e}{h_e})}\left[\left(\frac{m\pi}{L_x}\right)^2 + \left(\frac{n\pi}{L_y}\right)^2\right]. \quad (2)$$

Here ρ_{Al}, ρ_e, h_{Al}, and h_e are the densities and thicknesses of the Al and bath, respectively, and g is the magnitude of the gravitational acceleration. The electromagnetic forces couple certain modes with similar frequencies which amplify the perturbations [10, 16]. If strong enough, this coupling creates a circulating travelling wave that can grow exponentially in time until the Al shorts to the anode or the cell sloshes out of control [17]. In other words, when two wave modes have nearly identical frequencies and cause interface surface motion at right angles (e.g., one with $m = 0$ and another with $n = 0$), their resonant coupling via the electromagnetic force can give rise to the MPI [13].

Many methods for MPI suppression have been attempted in the past, including inserting baffles in the Al layer [6, 18] or tilting the anode in synchrony with interface motion [6], with limited success. In practice, the MPI is mitigated by building cells with greater length L_x than width L_y which would increase the separation between modes as shown by Eq. 2, by carefully designing the busbar network configuration to have a "better" vertical magnetic field (B_z) [19–21], and by keeping the ACD thick at the expense of reduced energy efficiency and increased carbon emissions. Recently, we showed [17] that adding an oscillating (AC) current component, with a particular frequency and amplitude, to the steady electrolysis current prevented the MPI in high fidelity simulations of a TRIMET 180 kA Al electrolysis cell [22]. The AC current excites standing wave modes which frustrate the MPI traveling wave [17]. Using this novel strategy could enable producing Al with less energy, lower cost, and lower emissions. The choice of AC current and frequency is of particular importance not only for the stabilization to be effective but also for this stabilization method to be commercially viable.

Stabilizing Electrolysis Cells

Simulating MPI

To study the stability of a typical Al electrolysis cell under the influence of an oscillating AC current, we used the simulation package MHD-Valdis, a tool used in the industry to design stable Al cells. MHD-Valdis has been described in detail [23]. It dynamically couples the transient turbulent motion of each fluid layer and the Al-bath interface shape to the transient magnetic field and electric currents in the cell [23]. The model includes essential commercial cell features such as the electrolyte channels [24], electric current distribution in the busbars, and the magnetic field generated by the ferromagnetic cell elements [23]. MHD-Valdis has been validated against a benchmark model [25], against measurements from the TRIMET 180 kA commercial potline [26], and against other commercial cells [27, 28]. A model of the same TRIMET 180 kA cell [22] is used in our study with Al-bath interface shape initialized with the $G_{1,0}$ gravity mode as a perturbation with an amplitude of $\alpha_{1,0} = 5$ mm, similar to previous work [26]. We use a 0.25 s time step and a numerical grid having $N_x \times N_y = 87 \times 31$ elements, so the grid size is 11.90×9.21 cm. Simulation is halted if the interface touches the anode, or after a set time has elapsed.

We first ran a series of simulations with steady 180-kA currents and varying ACD to find its critical value for stability. At the critical ACD, the motion of a point on the interface has an amplitude that neither grows nor decays in time. We quantified the Al-bath interface displacement by the root-mean-square (RMS) displacement of the interface from its mean as

$$z_{\mathrm{RMS}} = \left(\frac{1}{N_x N_y}\sum_{i=1}^{N_x}\sum_{j=1}^{N_y}(z_{i,j} - \overline{z_{i,j}})^2\right)^{\frac{1}{2}}, \quad (3)$$

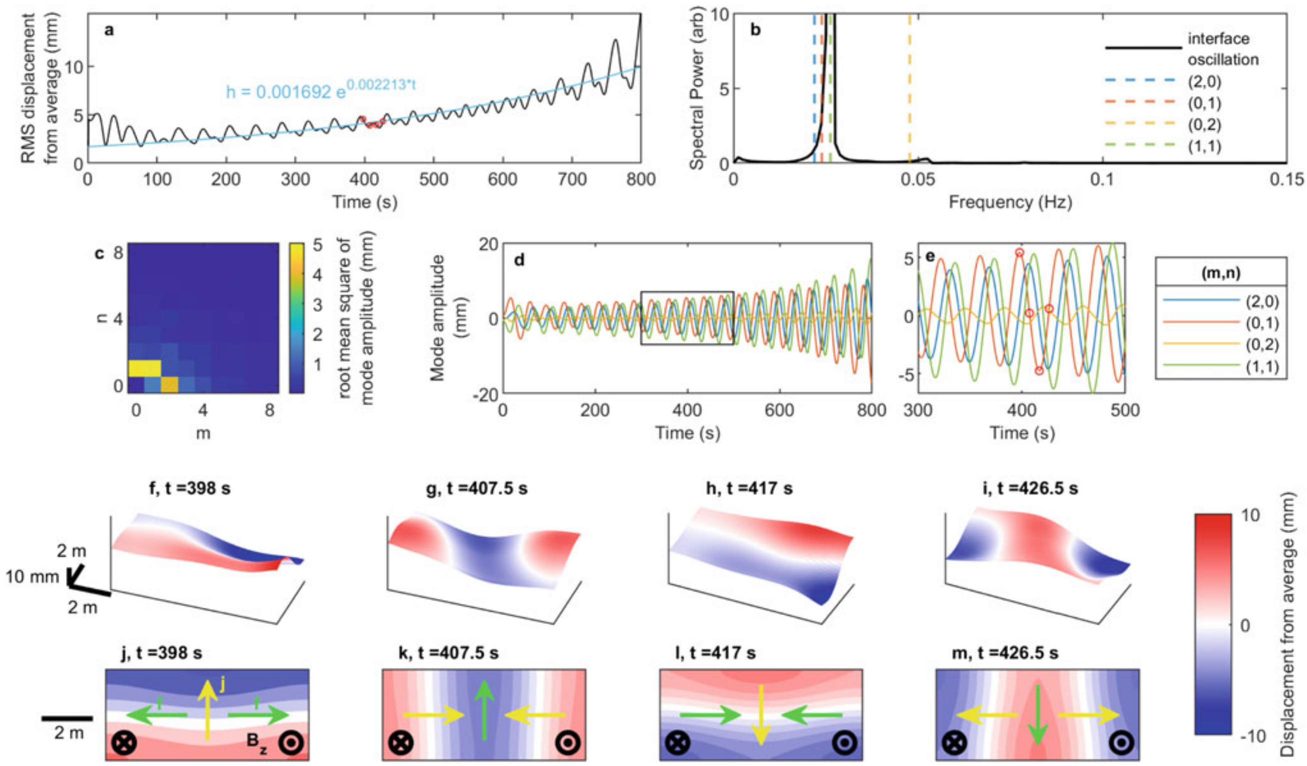

Fig. 2 The metal pad instability (MPI) in a simulated Al electrolysis cell. **a** Displacement of the Al-electrolyte interface grows exponentially, as shown by the fitted curve. **b** The spectral power of the displacement of one point on the interface is dominated by a narrow frequency band, close to the gravitational wave modes $G_{2,0}$, $G_{0,1}$, and $G_{1,1}$, expected in the MPI. **c** $G_{2,0}$, $G_{0,1}$, and $G_{1,1}$ have greater root-mean-square amplitude than any other modes. **d** $G_{2,0}$, $G_{0,1}$, $G_{1,1}$, and $G_{0,2}$ oscillate with a common frequency and grow over time. **e** $G_{2,0}$ and $G_{0,1}$ are separated in phase by $\sim 90°$, characteristic of a traveling wave as in the MPI. **f–i** Interface displacements at four times spanning one MPI cycle (red dots in (**e**)) show a circulating traveling wave. **j–m** Interface displacements at the same times as in (f–i), estimated using only $G_{2,0}$ and $G_{0,1}$ and viewed from above. The primary directions of the vertical magnetic field B_z, horizontal current j, and resulting electromagnetic forces f are sketched; their timing and arrangement are right for amplifying the circulating wave [17] (Color figure online)

where $z_{i,j}$ is the surface height of element (i, j), and $\overline{z_{i,j}}$ is its time-averaged height. The electromagnetic forces due to the current and B_z (Fig. 1a) cause the interface to bulge (Fig. 1b) as expected. We found the critical ACD to be at 4.3 cm, where the RMS interface displacement stably oscillates (Fig. 1c).

When the ACD is decreased by 7% to 4 cm, the MPI manifests, with z_{RMS} growing exponentially at a rate of 0.0022 s^{-1} (Fig. 2a). Oscillation was also evident, so we calculated the power spectrum of the displacement at a point, finding its power to be highly concentrated near 0.0263 Hz (Fig. 2b), close to $f_{2,0}$, $f_{0,1}$, and $f_{1,1}$, the frequencies of the modes whose coupling is expected to produce the MPI [13]. To verify the role of those three modes, we performed a least-squares projection of the simulated interface shape onto a basis set of gravity modes $G_{m,n}$, then calculated the RMS amplitude $\langle \alpha_{m,n} \rangle^{\frac{1}{2}}$ of each mode, through the duration of the simulation (Fig. 2c). As expected, $G_{2,0}$, $G_{0,1}$, and $G_{1,1}$ are far stronger than all other modes. Their amplitudes $\alpha_{m,n}$ grow exponentially over time and oscillate with frequencies near 0.0263 Hz (Fig. 2d, e). Visualizing the interface shape at four times spaced evenly through a 0.0263-Hz oscillation cycle reveals canonical MPI dynamics: a traveling wave that circulates counter-clockwise when viewed from above (Fig. 2f–i), consistent with the fact that $G_{2,0}$ and $G_{0,1}$ vary with $\sim 90°$ phase difference. The coupling between the three dominant modes, $G_{2,0}$, $G_{0,1}$, and $G_{1,1}$, relies on the different components of B_z and is explained in detail in [17]. Here, we only show the coupling between $G_{2,0}$ and $G_{0,1}$ which happens through the linear variation in the x direction of B_z (Fig. 2j–m). Current flows preferentially where the bath is thinner (interface crests), then spreads horizontally after entering the Al layer. Interacting with an ambient vertical magnetic field B_z that points upward at one end of the cell and downward at the other, horizontal current density j produces electromagnetic forces $f = j \times B_z$ that drive Al first along the x axis, then along the y axis, forming a closed cycle that amplifies the circulating traveling wave [8, 10, 13].

Adding AC Current

In another simulation, we found that the TRIMET 180 kA cell at 4 cm ACD can be successfully stabilized by adding an AC current of half-amplitude 19.8 kA (11% of the steady current) and frequency 0.045 Hz to the cell that seems to excite a standing wave that frustrates the MPI [17]. Though the RMS interface displacement oscillated, it did not grow exponentially (Fig. 3a). The spectral power of the interface displacement at a point showed strong peaks at two frequencies, one near $f_{2,0}$, $f_{0,1}$, and $f_{1,1}$, as seen in the presence of the MPI, and another near the 0.045 Hz AC current frequency (Fig. 3b). The AC current frequency of 0.045 Hz nearly matches the frequencies $f_{0,2}$ and $f_{4,0}$ of modes $G_{0,2}$ and $G_{4,0}$. Indeed, decomposing the interface shape into wave modes shows that $G_{0,2}$ and $G_{4,0}$ are strongest (Fig. 3c). The temporal variations of their amplitudes $\alpha_{m,n}$ are nearly sinusoidal (Fig. 3d–e). Visualizing the interface shape at four times spaced evenly through a 0.045 Hz oscillation cycle reveals not a traveling wave, as would occur with the MPI, but a standing wave (Fig. 3f–i), consistent with the fact that $G_{0,2}$ and $G_{4,0}$ vary synchronously and with almost no phase difference (Fig. 3e). The electromagnetic forces resulting from these standing waves seem to be stopping the MPI (Fig. 3j–m).

Having successfully suppressed the MPI and stabilized the Al cell with an oscillating AC current, at a specific amplitude and frequency, we wondered how changing the amplitude and the frequency would impact the cell. To investigate, we ran a series of simulations at 4 cm ACD, each with an AC current at a unique amplitude and frequency.

Results

AC Current Amplitude and Frequency

Using a lower AC current amplitude would probably be better to implement practically needing simpler electronics and is cheaper. So, we ran the same simulation, but with the AC amplitude decreased to 3.6 kA, 2% of the steady current, to check whether the cell would remain stable. Results shown in Fig. 4a indicate that the cell is unstable, with the RMS displacement growing exponentially. The spectral power of a point on the interface no longer shows the driving frequency of 0.045 Hz, but only the MPI frequency of 0.0263 Hz (Fig. 4b). However, the displacement growth rate 0.0021 s^{-1} is lower than in the case without AC current. This suggests that the AC current still has a stabilizing effect but not strong enough to stop the MPI. Thus, the minimum AC amplitude at which the cell is stable would be optimal.

Since oscillations drive standing waves, large oscillations might drive standing waves whose amplitude causes the Al layer to contact the anode, shorting the cell. To test that hypothesis, we ran a simulation with 20% AC amplitude. The cell shorted within 110 s, as shown (Fig. 5a, b).

Results in [17] show that the AC current frequency should be close to that of a hydrodynamic gravity mode. Since many wave modes are possible, we ran a simulation at 4 cm ACD but with the AC current having 11% amplitude and a very high frequency of 0.5 Hz, an order of magnitude higher than 0.045 Hz and nearly equal to high-order frequencies $f_{44,0}$ and $f_{0,20}$. The interface displacement grew exponentially in time (Fig. 6a) but at a lower rate than the case without AC current. The drive frequency of 0.5 Hz does not appear in the power spectrum of a point on the interface (Fig. 6b). We believe that the high-frequency oscillations were damped out by dissipative effects, such as the friction between the fluid layers and electrodes, and the turbulent viscosity [8, 10].

We ran another simulation with driving frequency 0.069 Hz, near the low-order frequency $f_{6,0}$. The cell was again stabilized, with the interface displacement only oscillating in time, not growing exponentially (Fig. 7a). The spectral power of a point on the interface shows two frequency peaks, one at the MPI frequency and the other near the driving frequency (Fig. 7b). Decomposing the interface displacement into the wave modes shows that $G_{0,2}$ is the most dominant followed by $G_{6,0}$ (Fig. 7c). The temporal variations of their amplitudes $\alpha_{m,n}$ are nearly sinusoidal (Fig. 7d–e). Visualizing the interface shape at four times spaced evenly through a 0.069 Hz oscillation cycle reveals a standing wave (Fig. 7f–i). $G_{0,2}$ and $G_{6,0}$ do vary with a phase difference unlike (Fig. 3e). The interface displacement is reconstructed using only the $G_{0,2}$ and $G_{6,0}$ (Fig. 7j–m). For a given AC current amplitude, it seems that cells can be more easily stabilized by exciting low-frequency modes than high-frequency modes.

Exciting Waves and Current Efficiency

Beyond energy efficiency, another key operational parameter for Al cells is current efficiency. The theoretical production rate in an Al cell can be found using Faraday's law for electrolysis:

$$p_0 = \frac{M}{zF} I, \tag{4}$$

where p_0 is the production rate in (g/s), M is the molecular mass in (g), z is the number of electrons involved in the reaction, F is the Faraday constant, and I is the electrolysis current. The theoretical production rate is proportional to the electrolysis current, and ideally, all the current should liberate Al atoms from solution. However, in reality "losses" occur where the current is instead, for example, driving back reactions or travelling short-circuit paths between the electrodes. These losses are typically quantified by the current efficiency

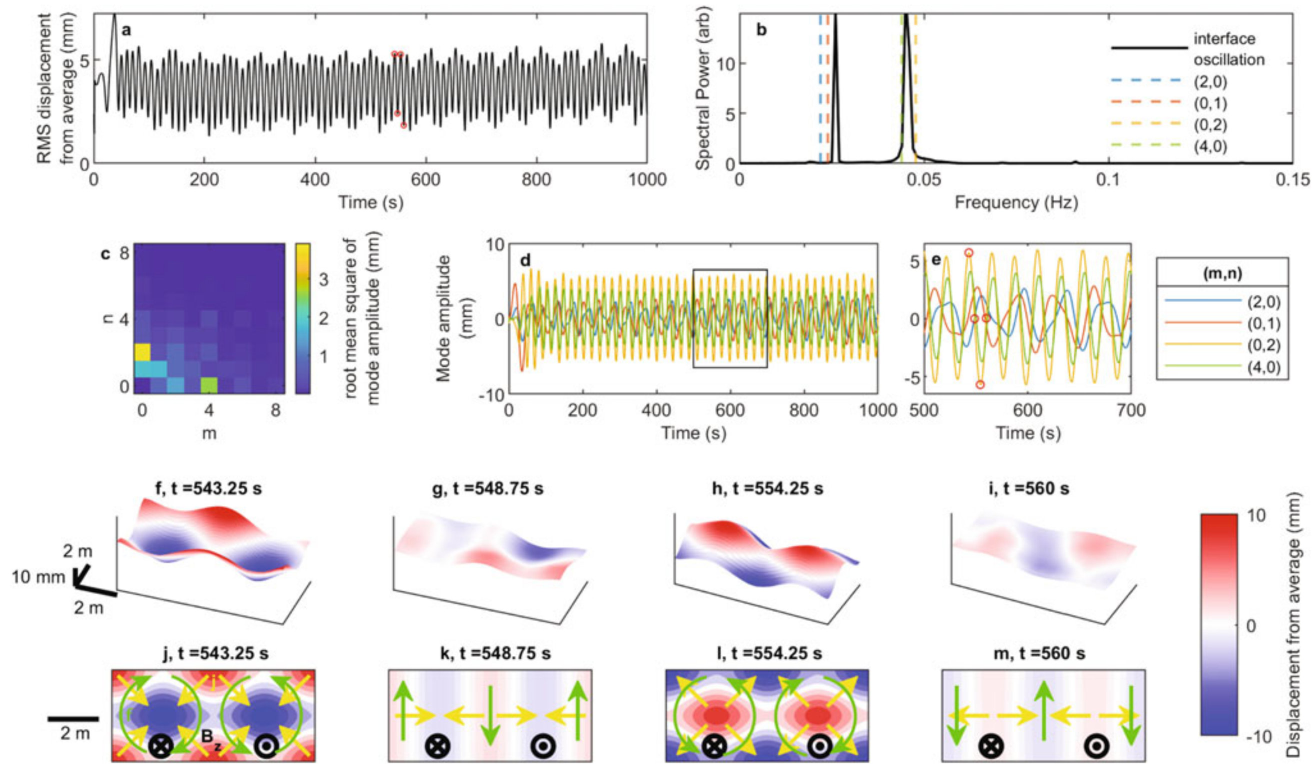

Fig. 3 An oscillating current component prevents the MPI. **a**, The Al-electrolyte interface oscillates stably. **b**, The spectral power of the displacement of one point on the interface is dominated by one frequency band close to the expected MPI frequency, and another close to the drive frequency. **c**, $G_{2,0}$, $G_{1,0}$, $G_{0,2}$, and $G_{4,0}$ have greater RMS amplitude than any other modes. **d–e**, Their amplitudes $\alpha_{m,n}$ oscillate, and $G_{0,2}$ and $G_{4,0}$ are almost aligned in phase, characteristic of a standing wave. **f–i**, Interface displacements at four times spanning one drive cycle (red dots in (**e**)) show a standing wave. **j–m**, Interface displacements at the same times as in (**f–i**), estimated using only $G_{0,2}$ and $G_{4,0}$ and viewed from above. The resulting electromagnetic forces f (sketched) often favour clockwise circulation, opposing and frustrating the MPI [17] (Color figure online)

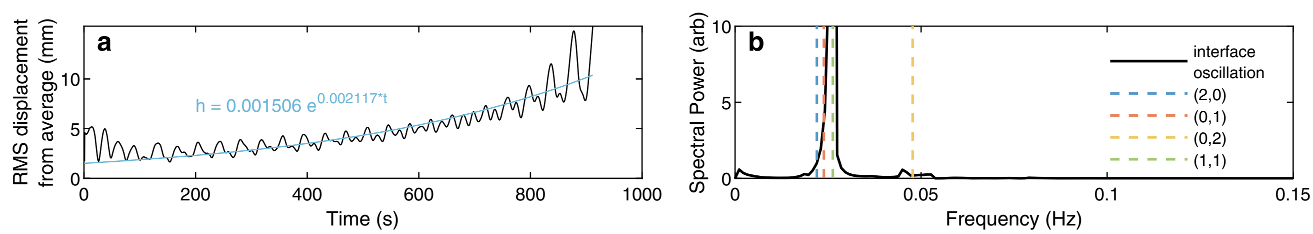

Fig. 4 A 2% AC current amplitude is not strong enough to stabilize the cell. **a** The Al-electrolyte interface grows exponentially. **b** The spectral power of the displacement of one point on the interface is dominated by one frequency band close to the expected MPI frequency

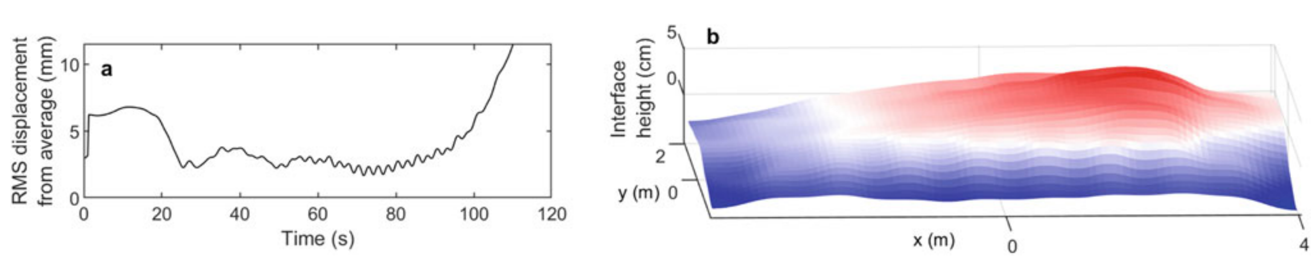

Fig. 5 A 20% AC current amplitude shorts the cell. **a** The Al-electrolyte interface grows exponentially until it reaches the anode and shorts the cell. **b** Al-bath interface at time 110 s, just before the cell shorted

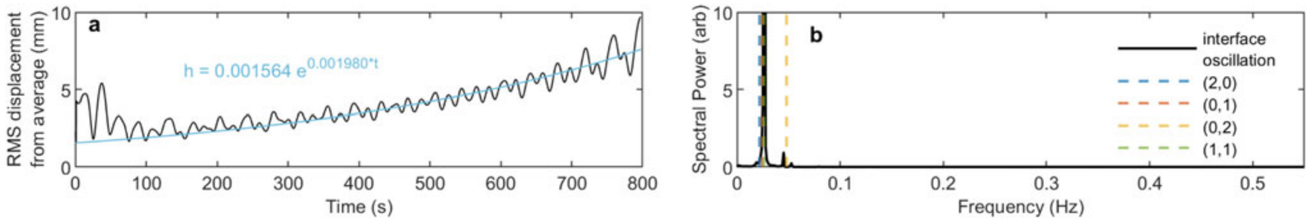

Fig. 6 High-frequency AC current has minimal effect. **a** When an 0.5 Hz oscillation is applied with 11% amplitude at 4 cm ACD, the Al-electrolyte interface grows exponentially, and the MPI is present. **b** The spectral power of the displacement of one point on the interface is dominated by one frequency band close to the expected MPI frequency. The driving frequency is absent

$$CE = \frac{p}{p_0} * 100\%, \quad (5)$$

where p is the measured production rate in (g/s). The biggest loss in CE comes from the back reaction occurring between the dissolved Al metal and carbon dioxide (CO_2) bubbles:

$$2Al + 3CO_2 = Al_2O_3 + 3CO. \quad (6)$$

This reaction is estimated to cause a ≈ 3–5% loss in CE [29]. A model of the reaction rate [29, 30] predicts the current efficiency to be

$$CE = 100\% - k_{Al}A(c^0_{Al} - c_{Al}), \quad (7)$$

where k_{Al} is the mass transfer coefficient between Al and bath, A is the surface area of the Al-bath interface, c^0_{Al} is the thermodynamic saturation solubility of Al in the bath, and c_{Al} is the amount of Al actually dissolved.

Because CE is inversely proportional to the surface area of the Al-bath interface as shown by Eq. 7, we wondered if driving standing waves, which increase surface area, might decrease CE. If $z = S(x, y, t)$ represents the interface, then its surface area can be calculated by

$$A(t) = \int_{-L_x/2}^{L_x/2} \int_{-L_y/2}^{L_y/2} \sqrt{S_x^2 + S_y^2 + 1}\, \mathrm{d}y\, \mathrm{d}x, \quad (8)$$

where S_x and S_y are the partial derivatives of $S(x, y, t)$ in the x and y directions, respectively. We numerically calculated the surface area of the interface given by Eq. 8 at every instant in time using MATLAB for different cell operating conditions. When the cell is stable with a steady 180 kA current at 4.3 cm ACD, the surface area of the interface oscillates in time about a mean value of 28.273 m^2 with an amplitude of 2 cm^2, a mere 0.0007% of the mean value (Fig. 8a). When the ACD is reduced by 7% to 4 cm and the cell is unstable with the MPI present, the surface area oscillates and grows in time (Fig. 8b) reaching a maximum value of 28.278 m^2 before the cell shorts. When we supplement the steady current, at 4 cm ACD, with an oscillating component of 19.8 kA amplitude and 0.045 Hz frequency to stabilize the cell, the surface area does not grow and only oscillates in time about a mean value of 28.2735 m^2 with an amplitude of ∼45 cm^2 (Fig. 8c). Both the mean area and the area oscillation are larger than at stable operation with a steady current, however, the change is not large enough to create a significant effect on CE.

CE is also inversely proportional to the mass transfer coefficient as shown in Eq. 7. Previous work in [31, 32] shows that decreasing the ACD will increase the mass transfer coefficient, thus decreasing CE. Reducing the ACD by 0.3 cm, from 4.3 cm to 4 cm, would perhaps decrease CE by a few percent [32]. Furthermore, by exciting standing waves to stabilize the Al cell, not only are the cells operating at a lower ACD but also with a higher wave amplitude. This combination is unfavorable for CE given the mechanism outlined in [32]. The gas bubbles travelling along the anode have thick fronts, and the high metal waves will collide with these bubbles inducing the back reaction and decreasing CE. Given a distribution for the gas bubbles and the waves on the Al-bath interface, having a lower ACD and higher waves would increase the overlapping area between the two distributions further decreasing CE.

Discussion

We simulated the Al-bath interface evolution for a TRIMET 180 kA Al reduction cells, used by TRIMET Aluminum, SE, in Germany. These cells normally operate at 4.5 cm ACD and have been simulated in previous studies that validated the model with real-world measurements [22, 26, 33]. The MPI imposes a critical ACD on Al cells, reducing their energy efficiency. Applying AC currents can prevent the MPI by exciting standing waves, and thus allows for squeezing the ACD below its critical threshold. The choice of the AC current frequency and amplitude will influence the effectiveness and commercial viability of using this method. Lower amplitudes are desirable but can make the stabilization effect too weak to stop the MPI, whereas high amplitudes can drive standing waves large enough to short the cell. This suggests that for a given frequency and ACD, the lowest amplitude

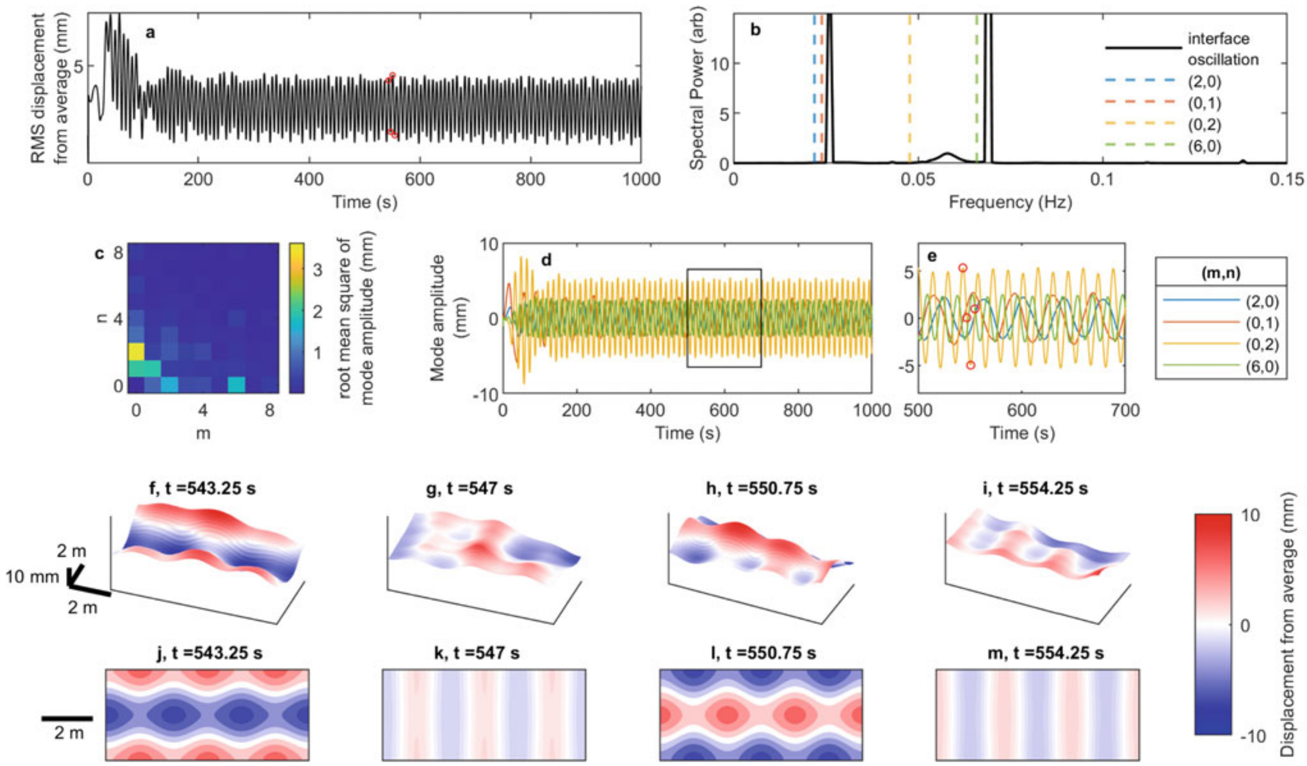

Fig. 7 An oscillating current component with frequency 0.069 Hz prevents the MPI. **a** The Al-electrolyte interface oscillates stably. **b** The spectral power of the displacement of one point on the interface is dominated by one frequency band close to the expected in the MPI frequency, and another close to the drive frequency. **c** $G_{2,0}$, $G_{0,1}$, $G_{0,2}$, and $G_{6,0}$ have greater root-mean-square amplitude than any other modes. **d–e** Their amplitudes $\alpha_{m,n}$ oscillate. **f–i** Interface displacements at four times spanning one drive cycle (red dots in (**e**)) show a standing wave. **j–m** Interface displacements at the same times as in (**f**–**i**), estimated using only $G_{0,2}$ and $G_{6,0}$ and viewed from above [17] (Color figure online)

that can stabilize the cell would be the best to use. To excite a standing wave, the drive frequency needs to be close to that of a hydrodynamic gravity mode. We showed that using an AC frequency near a high-frequency mode has almost no effect, likely because of the damping in the cell. Driving low-frequency modes seems to be very effective, and perhaps the lowest frequency mode has the strongest stabilization effect. For different cell designs, the frequencies of hydrodynamic gravity modes will be different, depending on cell dimensions, aspect ratio, and bath density. Identifying the best operating frequency can allow for more ACD reduction, or perhaps stable operation at a lower AC amplitude.

Using an AC current to stabilize Al cells excites standing waves on the Al-bath interface, allowing cell operation at lower ACD (4 cm vs. 4.3 cm). We showed that the excited waves have a higher amplitude than those at 4.3 cm ACD but the increase in surface area has little effect on CE. However, what is more important is decreasing the ACD while having an increased wave amplitude. This combination negatively impacts the cell's CE [32]. Additionally, the mass transfer coefficient k_{Al} in Eq. 7 depends on the material properties of the bath, the relative velocity between the Al and the bath, and the width of the reaction zone [29]. We expect that exciting standing waves at the interface would impact both the relative velocity and the reaction zone width. Incorporating such effects would improve our understanding of the impact exciting standing waves has on the cell's CE.

There are other limitations to our study. We have held constant both the thickness of the Al layer and the thickness of the ledge of frozen electrolyte at the cell wall, but their values vary and almost certainly affect cell stability and mode frequencies. Simulations with shorter time steps might allow resolving wave variation with greater detail (though the time scale for instability growth is much longer than the time step we have used). The simulations we conducted describe only magnetohydrodynamic aspects of the cell, not thermal aspects; coupling the interface displacement results with a simulation of the cell's energy balance [34] would give a more complete picture.

In future work, we hope to further investigate the amplitude-frequency phase space for a cell at a given ACD with more simulations, which could hint at the functional relationships among amplitude, frequency, and interface growth rate. Identifying these relationships would make the process of choosing the appropriate amplitude and frequency for the AC current more efficient. AC currents

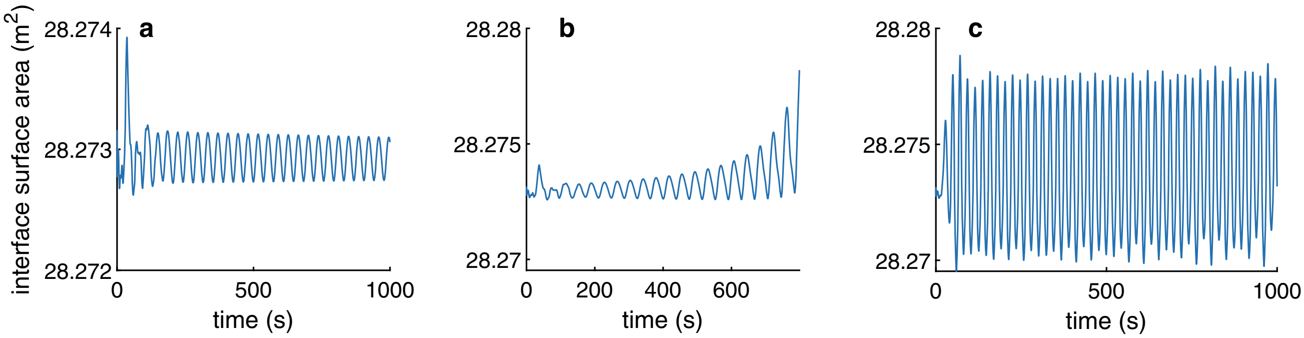

Fig. 8 Interface area in stable, unstable, and stabilized cells. **a** Al-electrolyte interface surface area as a function of time for a stable Al cell operating with a steady 180 kA current at 4.3 cm ACD. The surface area oscillates in time and decreases very slowly. **b** Interface surface area for a cell operating with a 180 kA current at 4 cm ACD. The surface area is growing in time, which is consistent with this cell being unstable. **c** Interface surface area for a cell operating with 180 kA steady current and an AC current with amplitude 19.8 kA and 0.045 Hz at 4 cm ACD. The surface area oscillates in time and does not grow but it is larger than that of panel **a**. This is consistent with cell being stable and the increase in surface area is due to the excited standing waves by the AC current

and standing waves could impact not only CE but also other operational parameters beyond CE, including the cell's thermodynamic equilibrium and heat balance. Future work might explore that impact. Future work might consider the effect of applying multiple oscillation frequencies, either simultaneously or sequentially. An economic analysis would be useful: producing the large oscillating currents that we have simulated will require power electronics of substantial cost, but we expect that in nearly all cases, achieving the same efficiency increase by busbar reconfiguration or pot redesign would cost far more. Finally, it is essential to test our strategy in an industrial-scale Al cell, which we hope to do soon.

References

1. International Aluminium Institute, "Statistics," 2020. https://international-aluminium.org/statistics/primary-aluminium-production/
2. B. P. "bp statistical review of world energy," report, 2020. https://www.bp.com/content/dam/bp/business-sites/en/global/corporate/pdfs/energy-economics/statistical-review/bp-stats-review-2020-full-report.pdf
3. M. Gautam, B. Pandey, and M. Agrawal, *Chapter 8 - Carbon Footprint of Aluminum Production: Emissions and Mitigation*, pp. 197–228. Elsevier Inc, 2018.
4. B. Gates, *How to Avoid a Climate Disaster: The Solutions We Have and The Breakthroughs We Need*. New York: Alfred a Knopf, 2021.
5. International Aluminium Institute, "Aluminium sector greenhouse gas pathways to 2050," report, 2021, https://international-aluminium.org/resource/aluminium-sector-greenhouse-gas-pathways-to-2050-2021/
6. P. A. Davidson, "Overcoming instabilities in aluminium reduction cells: a route to cheaper aluminium," *Materials science and technology*, vol. 16, no. 5, pp. 475–479, 2000.
7. T. Sele, "Instabilities of the metal surface in electrolytic alumina reduction cells," *Metallurgical Transactions B*, vol. 8, no. 4, pp. 613–618, 1977.
8. Bojarevics and M. V. Romerio, "Long waves instability of liquid-metal electrolyte interface in aluminum electrolysis cells - a generalization of sele criterion," *European journal of mechanics, B, Fluids*, vol. 13, no. 1, pp. 33–56, 1994.
9. P. Davidson, "An energy analysis of unstable, aluminium reduction cells," *European Journal of Mechanics B-fluids*, vol. 13, pp. 15–32, 1994.
10. P. A. Davidson and R. I. Lindsay, "Stability of interfacial waves in aluminium reduction cells," *Journal of Fluid Mechanics*, vol. 362, pp. 273–295, 1998.
11. O. Zikanov, A. Thess, P. Davidson, and D. Ziegler, "A new approach to numerical simulation of melt flows and interface instability in hall-héroult cells," *Metallurgical and Materials Transactions B*, vol. 31, pp. 1541–1550, 2000.
12. A. Lukyanov, G. El, and S. Molokov, "Instability of mhd-modified interfacial gravity waves revisited," *Physics letters. A*, vol. 290, no. 3, pp. 165–172, 2001.
13. N. Urata, "Wave mode coupling and instability in the internal wave in aluminum reduction cells," in *TMS Annual Meeting*, pp. 455–460, 2005.
14. N. Urata, "Magnetics and metal pad instability," in *Light Metals: Proceedings of Sessions, AIME Annual Meeting*, pp. 581–591, 1985.
15. J.-F. Gerbeau, C. Le Bris, and T. Lelièvre, *Mathematical methods for the magnetohydrodynamics of liquid metals*, vol. 9780198566656. Oxford: Oxford University Press, 2006.
16. A. D. Sneyd and A. Wang, "Interfacial instability due to mhd mode coupling in aluminium reduction cells," *Journal of fluid mechanics*, vol. 263, pp. 343–360, 1994.
17. I. Mohammad, M. Dupuis, P. D. Funkenbusch, and D. H. Kelley, "Oscillating currents stabilize aluminium cells for efficient, low carbon production," 2021.
18. A. Pedcenko, S. Molokov, and B. Bardet, "The effect of "wave breakers" on the magnetohydrodynamic instability in aluminum reduction cells," *Metallurgical and Materials Transactions B*, vol. 48, no. 1, pp. 6–10, 2017.
19. G. O. Linnerud, R. Huglen, and N. H. ASA, "Method for electrical connection and magnetic compensation of aluminium reduction cells, and a system for same," 2011.
20. C. et al., "Device for connection between very high intensity electrolysis cells for the production of aluminium comprising a supply circuit and an independent circuit for correcting the magnetic field," 1987.
21. M. Dupuis, J. Chaffy, and B. Langon, "A new aluminium electrolysis cell busbar network concept," 2015.

22. A. Lützerath, *High Frequency Power Modulation - TRIMET smelters provide primary control power for stabilizing the frequency in the electricity grid*, pp. 659–662. 01 2016.
23. V. Bojarevics and K. Pericleous, “Time dependent electric, magnetic and hydrodynamic interaction in aluminium electrolysis cells,” in *Fifth International Conference on CFD in the Process Industries CSIRO*, 2006.
24. V. Bojarevics and K. Pericleous, “Time dependent mhd models for aluminium reduction cells,” in *TMS Annual Meeting*, pp. 199–206, 2010.
25. V. Bojarevics and K. Pericleous, “Solutions for the metal-bath interface in aluminium electrolysis cells,” in *TMS Light Metals* (G. Bearne, ed.), pp. 569–574, 2009.
26. V. Bojarevics and J. W. Evans, *Mathematical Modelling of Hall-Héroult Pot Instability and Verification by Measurements of Anode Current Distribution*, pp. 783–788. Hoboken, NJ, USA: John Wiley & Sons, Inc, 2015.
27. V. Bojarevics, E. Radionov, and Y. Tretiyakov, *Anode Bottom Burnout Shape and Velocity Field Investigation in a High Amperage Electrolysis Cell*, pp. 551–556. 2018.
28. R. Shaoyong, Y. Feiya, M. Dupuis, V. Bojarevics, and Z. Jianfei, *Production Application Study on Magneto-Hydro-Dynamic Stability of a Large Prebaked Anode Aluminum Reduction Cell*, pp. 603–607. Hoboken, NJ, USA: John Wiley & Sons, Inc, 2013.
29. T. Foosnaes, K. Grjotheim, R. Huglen, H. Kvande, B. Lillebuen, T. Mellerud, and T. Naterstad, *Introduction to Aluminium Electrolysis Understanding the Hall-Heroult Process*, pp. 136–138. Aluminium-Verlag, 1993.
30. B. Lillebuen, S. Ytterdahl, R. Huglen, and K. Paulsen, “Current efficiency and back reaction in aluminium electrolysis,” *Electrochimica acta*, vol. 25, no. 2, pp. 131–137, 1980.
31. S. Rolseth, T. Muftuoglu, A. Solheim, J. Thonstad, “Current Efficiency at Short Anode-Cathode Distance in Aluminium Electrolysis,” *Light Metals*, pp. 517–523, 1986.
32. A. Solheim, “Current Efficiency in Aluminium Reduction Cells: Theories, Models, Concepts, and Speculations,” *Light Metals 2014*, pp. 753–758, 2014.
33. M. Dupuis and V. Bojarevics, “Analyzing the impact on the cell stability power modulation on a scale of minutes,” in *Aluminium Smelting Industry*, pp. 54–57, 2021.
34. M. Dupuis, *How to Limit the Heat Loss of Anode Stubs and Cathode Collector Bars in Order to Reduce Cell Energy Consumption*, pp. 521–531. 01 2019.